

## RESEARCH ARTICLE

10.1002/2016WR019753

# Rescaling the complementary relationship for land surface evaporation

R. Crago<sup>1</sup>, J. Szilagyi<sup>2,3</sup>, R. Qualls<sup>4</sup>, and J. Huntington<sup>5</sup>

### Key Points:

- The complementary relationship needs to be rescaled on a daily basis
- Rescaling the CR reduces scatter and increases accuracy of actual evaporation estimates
- A new CR, based on rescaling, is developed

### Correspondence to:

R. Crago,  
rcrago@bucknell.edu

### Citation:

Crago, R., J. Szilagyi, R. Qualls, and J. Huntington (2016), Rescaling the complementary relationship for land surface evaporation, *Water Resour. Res.*, 52, 8461–8471, doi:10.1002/2016WR019753.

Received 10 SEP 2016

Accepted 18 OCT 2016

Accepted article online 22 OCT 2016

Published online 9 NOV 2016

<sup>1</sup>Department of Civil and Environmental Engineering, Bucknell University, Lewisburg, Pennsylvania, USA, <sup>2</sup>Department of Hydraulic and Water Resources Engineering, Budapest University of Technology and Economics, Budapest, Hungary, <sup>3</sup>Conservation and Survey Division, School of Natural Resources, University of Nebraska-Lincoln, Lincoln, Nebraska, USA, <sup>4</sup>Department of Biological Engineering, University of Idaho, Moscow, Idaho, USA, <sup>5</sup>Division of Hydrologic Sciences, Desert Research Institute, Reno, Nevada, USA

**Abstract** Recent research into the complementary relationship (CR) between actual and apparent potential evaporation has resulted in numerous alternative forms for the CR. Inspired by Brutsaert (2015), who derived a general CR in the form  $y = \text{function}(x)$ , where  $x$  is the ratio of potential evaporation to apparent potential evaporation and  $y$  is the ratio of actual to apparent potential evaporation, an equation is proposed to calculate the value of  $x$  at which  $y$  goes to zero, denoted  $x_{min}$ . The value of  $x_{min}$  varies even at an individual observation site, but can be calculated using only the data required for the Penman (1948) equation as expressed here, so no calibration of  $x_{min}$  is required. It is shown that the scatter in  $x$ - $y$  plots using experimental data is reduced when  $x$  is replaced by  $X = (x - x_{min}) / (1 - x_{min})$ . This rescaling results in data falling along the line  $y = X$ , which is proposed as a new version of the CR. While a reinterpretation of the fundamental boundary conditions proposed by Brutsaert (2015) is required, the physical constraints behind them are still met. An alternative formulation relating  $y$  to  $X$  is also discussed.

## 1. Introduction

Land surface evaporation and transpiration (referred to herein simply as “evaporation”) provides a key link between the land surface water and energy budgets. Some two-thirds of continental precipitation evaporates before reaching the ocean [Dingman, 2015], and globally slightly over half of the land surface net radiation goes toward vaporizing liquid water or ice [Brutsaert, 2005]. Despite its importance, land surface evaporation is difficult to estimate accurately using routine meteorological measurements. A number of approaches have been suggested, many of which rely on the land surface energy budget by either employing remotely sensed surface temperatures [e.g., Nishida et al., 2003; Bastiaanssen et al., 1998; see also Crago and Qualls, 2013] or converting potential evaporation estimates from the Penman [1948] or Priestley and Taylor [1972] equations to actual evaporation, often using some sort of stomatal or bulk surface resistance [e.g., Shuttleworth and Wallace, 1985; Shuttleworth and Gurney, 1990; Monteith and Unsworth, 2013]. These methods require either detailed spatial patterns of land temperature or information regarding the availability of moisture at the land surface.

The Complementary Relationship (CR) between actual and “apparent potential evaporation” (such as pan evaporation) has become an important tool for deriving evaporation rates from minimal data. First proposed by Bouchet [1963], the CR is also based on the energy budget, but it infers the dryness of the land surface from the aridity of the air. Over a homogeneous region experiencing minimal advection, the lower atmosphere is expected to be adjusted to the condition of the underlying surface, so that the humidity of the overlying air reflects the evaporation rate. Thus, low humidity in the surface layer of the atmosphere implies a low regional evaporation rate, while at the same time implying a high potential for evaporation. Thus, high apparent potential evaporation implies low actual regional evaporation and vice versa; they are complementary. Because of this interplay between actual and apparent potential evaporation, CR-based methods do not need information on moisture availability at the surface.

A wide range of complementary relationships has been proposed and applied over a wide range of land surfaces [e.g., Bouchet, 1963; Morton, 1983; Granger, 1989; Qualls and Gultekin, 1997; Ramirez et al., 2005;

Crago and Crowley, 2005; Kahler and Brutsaert, 2006; Szilagyi, 2007; Szilagyi and Jozsa, 2008; Pettijohn and Salvucci, 2009; Huntington et al., 2011; Han et al., 2012; Crago and Qualls, 2013; Hobbins et al., 2016; McEvoy et al., 2016]. The CR has also played a pivotal role in examining the “evaporation paradox,” namely, that global warming is expected to increase evaporation, while global pan evaporation rates have actually been decreasing in recent decades. Brutsaert and Parlange [1998] invoked the CR, arguing that as actual evaporation increases, atmospheric humidity increases, thus reducing the apparent potential evaporation, reflected in reduced pan evaporation [cf., Roderick et al., 2009a, 2009b]. As an example of the ability of the CR to estimate evaporation over a wide range of surfaces and climates, Szilagyi [2015] applied a CR-based method to estimate 30 year normal monthly evaporation rates over the conterminous United States. Required data included net radiation, wind speed, air temperature, and dew point temperature. Comparisons between the CR method evaporation and that derived from subtracting runoff from precipitation for 334 United States Geological Survey gaged watersheds spanning the country were compelling. For example the correlation coefficient was 0.95. Szilagyi [2015] noted that these results were “on par with the latest Land Surface Model results but without the need for soil and vegetation information or any soil moisture budgeting.”

Despite the widespread use of the method and its evident successes, one criticism of the CR has been the lack of a definitive derivation of it, although developments by Bouchet [1963] and many others [e.g., Morton, 1983; Granger, 1989; Brutsaert, 2005; Szilagyi, 2007; Aminzadeh et al., 2016] have attempted to correct this. Brutsaert [2015] provides a very general, as well as insightful, derivation of a CR. Drawing on his decades of contributions to the CR literature, his paper challenged the previous status quo and powerfully laid out a new state of the science, which any future studies will need to address. Since his work so clearly defined a theoretical framework and provided the definitions of the terms used herein, we will start with a brief review of his paper. We will show a weakness in his formulation, leading to a new form for the CR. Finally we will apply the new CR to several data sets and discuss the results and the implications of the new CR.

## 2. Background

First, Brutsaert [2015] carefully defined actual, potential, and apparent potential evaporation. Actual evaporation ( $E$ ) is the surface water vapor (or latent heat) transport rate from a large uniform region where any edge effects are small because of its size and homogeneity. Potential evaporation ( $E_{p0}$ ) is the evaporation rate this same region would have if net radiation at the surface was the same but the surface was saturated, so that the air in contact with the skin of the surface was saturated. It is implied that the lower atmosphere has fully adjusted to this saturated surface. Further,  $E$  depends on the same variables as  $E_{p0}$ , except  $E$  adds an additional variable related to the availability of water at the surface. Apparent potential evaporation ( $E_{pa}$ ) is “the evaporation that would take place from a small saturated surface inside the larger surface. . .subject to the same non-potential atmospheric conditions.” This surface is small enough that it does not affect the humidity or the evaporation rate from the surrounding area [Brutsaert, 2015]. Note that  $E$ ,  $E_{p0}$ , and  $E_{pa}$  are here expressed in energy units ( $W m^{-2}$ ).

Brutsaert [2015] noted that for a saturated surface,  $E = E_{p0} = E_{pa}$ , but as the surface dries,  $E$  decreases while  $E_{pa}$  increases. Thus,  $E \leq E_{p0} \leq E_{pa}$ . He introduced nondimensional  $E_{p0}$  and  $E$  via dividing them by  $E_{pa}$ :  $x = E_{p0}/E_{pa}$  and  $y = E/E_{pa}$ . When  $E$  decreases below  $E_{p0}$  due to a nonsaturated surface,  $E_{p0} - E = \Delta Q$ , or nondimensionally,

$$x - y = \frac{\Delta Q}{E_{pa}} \tag{1}$$

where  $\Delta Q$  is the amount  $E$  has decreased below  $E_{p0}$ . As a response,  $E_{pa}$  increases above  $E_{p0}$  by an amount dependent on  $\Delta Q/E_{pa}$ . Nondimensionally, this is written

$$1 - x = f(\Delta Q/E_{pa}) \tag{2}$$

Equations (1) and (2) can be combined to yield

$$y = x - F(1 - x) \tag{3}$$

where  $F(\ )$  is the inverse of  $f(\ )$ . By expressing  $F$  as a polynomial, he arrives at

$$y = x - \sum_{i=0}^n a_i x^i \tag{4}$$

where the  $a_i$ 's are coefficients and  $n$  is the order of the polynomial.

Equation (4) is a general CR relationship. To develop a useful equation, *Brutsaert* [2015] imposed four physically determined boundary conditions which he used with (4) to develop a fourth-order polynomial solution. Specifically, he required that: (i)  $y = 1$  at  $x = 1$ ; (ii)  $y = 0$  at  $x = 0$ ; (iii)  $dy/dx = 1$  at  $x = 1$ ; and  $dy/dx = 0$  at  $x = 0$ . This resulted in the complementary relationship

$$y = (2 - c)x^2 - (1 - 2c)x^3 - cx^4 \tag{5}$$

where  $c$  is a parameter which is ideally equal to zero, but can also be adjusted to account for various degrees of asymmetry in the complementary relationship. Values of  $y$  found using (5) will be denoted by  $y_B$  from here on.

Like *Brutsaert* [2015], and as first proposed by *Brutsaert and Stricker* [1979], we will assume that  $E_{p0}$  is given by the *Priestley and Taylor* [1972] equation and  $E_{pa}$  by the *Penman* [1948] equation. That is,

$$E_{p0} = \alpha \frac{\Delta}{\Delta + \gamma} (R_n - G) \tag{6}$$

where  $R_n$  is the net radiation,  $G$  is the ground heat flux,  $\alpha$  is the Priestley-Taylor parameter,  $\Delta$  is the slope of the saturation vapor pressure curve, and  $\gamma$  is the psychrometric constant. Also,

$$E_{pa} = \frac{\Delta}{\Delta + \gamma} (R_n - G) + \frac{\gamma}{\Delta + \gamma} L_e f_w(u) (e_a^* - e_a) \tag{7}$$

where  $L_e$  is the latent heat of evaporation,  $f_w(u)$  is a wind function,  $e_a^*$  is the saturated vapor pressure at the air temperature, and  $e_a$  is the measured vapor pressure of the air. As shown by *Brutsaert* [1982, 2005, 2015], the wind function  $f_w(u)$  can be formulated using similarity theory in terms of the measurement height  $z$ , the displacement height  $d_o$ , the roughness length for momentum  $z_o$ , and water vapor  $z_{ov}$ . The wind function  $f_w(u)$  is defined by

$$f_w(u_1) = \frac{0.622k^2 u_1}{R_d T_a \ln \left[ \frac{(z_2 - d_o)}{z_{ov}} \right] \ln \left[ \frac{(z_1 - d_o)}{z_o} \right]} \tag{8}$$

where  $k = 0.4$  is von Karman's constant,  $R_d$  is the ideal gas constant for air,  $u_1$  is the horizontal wind speed measured at height  $z_1$ , and  $e_a$  in (7) and the absolute air temperature  $T_a$  in (8) (from which  $e_a^*$  is also calculated) are measured at  $z_2$ . The term  $L_e f_w(u) (e_a^* - e_a)$  in (7) is commonly called the drying power of the air,  $E_d$ . Note that  $\Delta$  in (7) must be evaluated at  $T_a$ , while in (6) it must be evaluated at the wet surface temperature [*Szilagyi*, 2014], discussed below.

Since  $E_{p0}$  and  $E_{pa}$  are defined by (6) and (7), respectively, the models employed here can be considered variations of the Advection-Aridity approach of *Brutsaert and Stricker* [1979].

### 3. Theoretical Development

This project began with the framework of *Brutsaert* [2015] outlined in the previous section. In this section, we will show why his boundary condition (ii) needs to be modified, propose a modification, and suggest a new form of the CR that takes this new boundary condition into account.

We note that  $y \rightarrow 0$  when  $E \rightarrow 0$ . When  $E_{pa}$  is estimated with the *Penman* equation it cannot become infinite, because both the available energy and the drying power of the air are finite, even when the vapor pressure of the air is zero. Evaporation from a finite-sized wet surface cannot become infinite for the same reason—both energy and drying power are limited. We expect that  $y \rightarrow 0$  at some value  $x = x_{min}$ , where  $x_{min}$  must be between 0 and 1 [*Szilagyi et al.*, 2016]. The variable  $x_{min}$  is the value of  $x = E_{p0}/E_{pa}$  corresponding to a value of  $y = E/E_{pa} = 0$ . Therefore,  $y$  reaches zero only when  $x$  reaches the smallest value possible for a given  $E_{p0}$ . It could be assumed that  $x_{min}$  is a constant, but close examination of the concept of  $x_{min}$  shows that this is only an approximation. We expect that  $x = E_{p0}/E_{pa}$  reaches its minimum physically realistic value,

$x_{min}$ , only when  $E_{pa}$  is at its maximum value (except for the obvious exception when  $E_{p0} = 0$ , in which case  $x_{min} = 0$ ). The question is then how to determine the maximum value of  $E_{pa}$ —the value  $E_{pa}$  would have if the regional surface was devoid of all moisture—which will be denoted  $E_{pads}$  (that is, the hypothetical  $E_{pa}$  for a dry surface).

The wet surface temperature,  $T_{ws}$  is the temperature of the saturated air contacting the skin of the wet surface (such as a sunken evaporation pan) [Szilagyi and Jozsa, 2008; Szilagyi, 2014, 2015]. Szilagyi and Jozsa [2008] showed that  $T_{ws}$  can be calculated based on actual available energy and air temperature along with  $E_{pa}$  calculated for the actual conditions. The method is based on the Bowen ratio  $B_o$  (ratio of sensible to latent heat flux) applied for a small wet surface:

$$B_o = \frac{(R_n - G) - E_{pa}}{E_{pa}} \approx \gamma \frac{T_{ws} - T_a}{e^*(T_{ws}) - e(T_a)} \tag{9}$$

where  $T_a$  is the air temperature,  $e^*(T_{ws})$  is the saturation vapor pressure at temperature  $T_{ws}$ , and  $e(T_a)$  is the actual vapor pressure of the air. Equation (9) is solved iteratively. Should  $T_{ws}$  from (9) exceed  $T_a$ , then  $T_{ws}$  is set to equal  $T_a$  [e.g., Szilagyi et al., 2016]. Szilagyi and Schepers [2014] have shown that  $T_{ws}$  remains constant during drying if net radiation and wind speed remain constant. This is significant here because  $T_{ws}$  should remain the temperature of the wet surface even when all the available moisture at the regional surface has been evaporated.

The maximum value of  $E_{pa}$  that can be obtained from this small wet surface, holding available energy, wind speed, and  $T_{ws}$  constant, would occur when the air in the surface layer above the wet surface is completely dry and the wet spot evaporates according to the aerodynamic mass transfer equation [e.g., Brutsaert, 1982]:

$$E_{pads} = \frac{L_e [q^*(T_{ws}) - 0] k \rho u_*}{\ln \left( \frac{z - d_0}{z_{ov}} \right)} \tag{10}$$

where  $q^*(T_{ws})$  is saturated specific humidity evaluated at  $T_{ws}$ ,  $\rho$  is the density of the air, and  $u_*$  is the friction velocity. Friction velocity is estimated by:

$$u_* = \frac{k u_1}{\ln \left( \frac{z_1 - d_0}{z_0} \right)} \tag{11}$$

Thus,  $E_{pads}$  is the theoretical evaporation rate from the saturated surface at a temperature  $T_{ws}$  up to a height great enough that the specific humidity has fully adjusted to the underlying regional surface of zero evaporation, rather than to the small wet patch. The specific humidity,  $q$ , is 0 at height  $z$  because regionally there is no source of moisture at the surface when  $y$  is zero. While available energy does not appear explicitly in (10) and (11), the estimation of  $T_{ws}$  assumes it remains constant. Because  $E_{pa}$  from (7) with (8) assumes similarity theory, and thus one-dimensional mass transfer from the surface,  $E_{pads}$  (the maximum possible value of  $E_{pa}$ ) also must assume one-dimensional transfer as in (10) and (11).

Since stability is not included in (10), a value of  $z$  relatively near the ground should be used; the present results use  $z = 2$  m. Equation (10) is largely a function of: (i)  $u_*$ ; (ii)  $(z - d_0)/z_{ov}$ ; and; (iii)  $T_{ws}$ . Note that this method has been developed for daily or longer duration estimates; at shorter durations alternative methods for estimating  $T_{ws}$  and  $E_{pads}$  would be required; in particular, stability would need to be accounted for.

Once  $E_{pads}$  has been determined,  $x_{min}$  is given by

$$x_{min} = \frac{E_{p0}}{E_{pads}} \tag{12}$$

The variable  $\Delta$  in  $E_{p0}$  and  $L_e$  in (10) are both calculated at temperature  $T_{ws}$ . Note that, for a given location and land cover,  $x_{min}$  is expected to vary primarily with wind speed and with available energy, since  $E_{p0}$  is primarily a function of available energy and  $E_{pads}$  is largely a function of the efficiency of mass transfer.

Since (12) provides a way to estimate the value of  $x$  where  $y \rightarrow 0$ , it would seem that the range of  $x$  values allowable for any given data point varies with  $x_{min}$ . This suggests that the CR might use  $x = x_{min}$  rather than  $x = 0$  as its lower boundary, so that the CR could be formulated by rescaling the  $x$  axis using

$$X = \frac{(x - x_{\min})}{(1 - x_{\min})} \quad (13)$$

One possible way to formulate a CR is to use

$$y = X \quad (14)$$

Considerations supporting (13) and (14) will be discussed in a later section.

As *Brutsaert* [2015] showed, the CR can be most compactly expressed in dimensionless form, and the dimensionless ratios represented by  $x$  and  $y$  both vary between the theoretical limits of 0 and 1 with this dimensionless form. Ultimately, however, a CR should be able to provide accurate estimates of evaporation, for example in latent heat flux units. Both  $E$  and  $y = E/E_{pa}$  will be considered here.

#### 4. Data and Calibration

Data came from the First ISLSCP (International Satellite Land Surface Climatology Project) Field Experiment (FIFE) in 1987 and 1989, Cooperative Atmosphere-Surface Exchange Study (CASES) in 1997, and the Basin and Range Carbonate-Rock Aquifer System (BARCAS) study described by *Moreo et al.* [2007] and *Huntington et al.* [2011].

The FIFE experiment took place in a hilly grassland in Kansas, USA [*Sellers et al.*, 1992], largely in the Konza Prairie natural area. Leaf area indices of the grassland sites typically ranged from 0.3 to 2.0 and canopy height ranged from 0.19 to 0.65 m. Portable Automated Mesonet II (PAM II) stations and colocated flux stations were distributed over the region. The PAM II stations measured temperature, humidity, and wind speed, while the flux stations measured net radiation, ground heat flux, and sensible and latent heat fluxes. For the FIFE 1987 experiment, the "surface flux baseline" data derived by *Sellers* [1994] were used. These data consist of the averages of all of the 21 flux stations that reported measurements for a given half-hour period. Both eddy covariance and Bowen ratio stations were included in the averages. See *Crago and Suleiman* [2005] and *Crago and Crowley* [2005] for further description. The FIFE 1989 data came from a single Energy Budget with Bowen Ratio (EBBR) station (station 944) operated by L. Fritschen; both the 1987 and 1989 data were downloaded from <https://daac.ornl.gov/FIFE/>. The spatially averaged 1987 data and the single-station 1989 data are treated here as separate experiments.

The CASES 1997 data came from a single site in a grassy field located in the Walnut River watershed in Kansas, USA and operated by R. Qualls. Surface fluxes were measured with the eddy covariance method. Net radiation, ground heat flux, sensible and latent heat fluxes, air temperature, air humidity, wind speed, and canopy height and density data were all available. Further description of the site and equipment can be found in *Crago and Crowley* [2005].

The data from the BARCAS study in eastern Nevada come from five eddy covariance stations located in sparsely vegetated shrublands. The climates ranged from arid to semiarid. Sensible and latent heat fluxes, net radiation, air temperature and humidity, and wind speed were all measured. Average energy balance closure errors were 10 percent, so a 10 percent adjustment was applied to the measured latent heat fluxes to account for this. Data from March through November of 2005, 2006, and 2007 were used. Details of the sites and equipment are given by *Moreo et al.* [2007].

For each of the experiments, sensible and latent heat fluxes, net radiation, ground heat flux, wind speed, air temperature, and humidity were recorded at 15–30 min time steps. These were converted into daily values following the averaging procedures outlined by *Allen et al.* [1998]. The BARCAS data were further processed into 10 day averages at each site. All the BARCAS results presented here are based on these 10 day averages. The parameters describing the roughness of each surface were taken as functions of the canopy height  $h$  as:  $z_0 = h/8$ ;  $d_0 = 2h/3$ ; and  $z_{0v} = z_0/10$  [see *Allen et al.*, 1998, Chapter 2, Box 4; *Brutsaert*, 2005, page 46]. Due to the patchiness of the shrubs at the BARCAS sites, the resulting values of  $z_0$  were multiplied by a coefficient  $m$ , which ranged from 0 to 1. It was assumed that  $m = 1$  for the other experiments.

Values of  $x$  and  $y$  were calculated for each of the four experimental data sets. That is,  $x$  was found from the ratio of  $E_{po}$  from (6) to  $E_{pa}$  from (7) with (8);  $y$  was found from the ratio of measured values of  $E$  ( $E_{ref}$ ) divided by  $E_{pa}$  from (7) with (8). The upper elevation for the calculation of  $E_{pads}$  (equation (10)) was taken at  $z = 2$  m.

The Priestley-Taylor  $\alpha$  and the parameter  $c$  in (5) were treated as calibration parameters for all the experiments, and  $m$  was also calibrated for the BARCAS data. Brutsaert [2005] stated that  $\alpha$  for saturated surfaces typically falls between 1.20 and 1.30, while Kahler and Brutsaert [2006] and Brutsaert [2015] used  $\alpha$  near 1.13. To accommodate the observed range of this parameter, here we assume  $1.10 \leq \alpha \leq 1.30$ . Szilagyi et al. [2016] noted that  $c$  is limited to the range  $-1 \leq c \leq 2$  to ensure that  $y$  increases monotonically with  $x$  and that  $y \leq x$  for  $0 \leq x \leq 1$ .

When  $\alpha$ ,  $c$ , and  $m$  are calibrated to optimize performance of (14) for the original, unscaled  $E$  using the method described in the next paragraph, the resulting values of  $E_{p0}$  and  $E_{pa}$  will be denoted  $E_{p01}$  and  $E_{pa1}$ , which are used to calculate values of  $x$  and  $y$  denoted  $x_1$  and  $y_1$ , respectively. When (5) is used in the optimization of the parameters, the corresponding variables will be denoted  $E_{p02}$ ,  $E_{pa2}$ ,  $x_2$ , and  $y_2$ . When discussing values of  $x$ ,  $y$ ,  $E_{p0}$ , or  $E_{pa}$  in general, without specifying the parameter values, the numerical subscripts will be omitted. Finally, the estimated evaporation rate  $X^*E_{pa1}$  will be denoted  $E_{X1}$  and  $y_B^*E_{pa2}$  will be denoted  $E_B$ .

Optimal values of  $\alpha$  and  $m$  for use with equation (14) are found by minimizing the root mean square difference (RMSD) between measured values of actual evaporation  $E_{ref}$  and  $E_X$ . Parameter values for use with (5) minimize RMSD between  $E_{ref}$  and  $E_B$ . Separate parameter values were obtained for each experiment and for each of the CR equations used (equations (5) and (14)). This calibration process ensured that each equation was given the physically realistic parameter values that allowed it to perform at its best. In this way, differences in performance between the equations are due to the inherent potential or limitations of the formulations rather than to arbitrary parameter values.

### 5. Results

Table 1 provides the parameter values obtained with the calibration process described above. Figure 1a plots  $x_1$  versus  $y_1$  for all the data sets. In the present Figure 1a, similar to Figure 1 in Brutsaert [2015], the vast majority of the points fall below the line  $y_1 = x_1$ , as required by the fact that actual evaporation should not exceed the apparent potential evaporation. Figure 1b shows the corresponding graph of  $x_2$  and  $y_2$ . The fact that the data clouds in our Figures 1a and 1b occupy similar regions on their respective graphs as Figure 1 of Brutsaert [2015], gives us some confidence that the values of  $\alpha$  and  $m$  found during the calibrations are appropriate.

**Table 1.** Values of Optimized Parameters and Model Performance Statistics, Where  $n$  is the Number of Data Points,  $R$  is the Correlation Coefficient,  $RMSD$  is the Root Mean Square Difference, and  $S$  and  $I$  are Defined by the Linear Regression Line  $y = S*y_{estimated} + I$ , Where  $y_{estimated}$  is Either  $y_B$  or  $X$

Method	Parameters	FIFE87 $n = 45$	FIFE89 $n = 15$	CASES $n = 13$	BARCAS $n = 282$	
Equation (14), $y_1 = X$	$a$	1.30	1.17	1.30	1.10	
	$m$	1	1	1	0.025	
	Statistics					
	$R(E_X, E_{ref})$	0.92	0.90	0.87	0.81	
	$R(X, y_1)$	0.89	0.94	0.88	0.82	
	$R(x_1, y_1)$	0.83	0.93	0.84	0.63	
	$RMSD(E_X, E_{ref})$ ( $W\ m^{-2}$ )	20.6	13.3	14.8	8.7	
	$RMSD(X, y_1)$	0.093	0.081	0.068	0.095	
	$S$	0.86	1.19	0.81	0.77	
	$I$	0.07	-0.11	-0.11	0.13	
	Equation (5), $y_2 = y_B$	Parameters				
$a$		1.30	1.22	1.30	1.10	
$m$		1	1	1	0.40	
$c$		-0.14	0.05	0.14	1.1	
Statistics						
$R(E_B, E_{ref})$		0.76	0.86	0.80	0.76	
$R(y_B, y_2)$		0.82	0.93	0.84	0.75	
$R(x_2, y_2)$		0.83	0.93	0.84	0.71	
$R(X, y_2)$		0.89	0.94	0.88	0.83	
$RMSD(E_B, E_{ref})$ ( $W\ m^{-2}$ )		35.1	14.7	17.1	9.2	
$RMSD(y_B, y_2)$		0.152	0.081	0.092	0.075	
$S$	0.61	1.04	0.63	0.76		
$I$	0.18	-0.03	0.18	0.24		

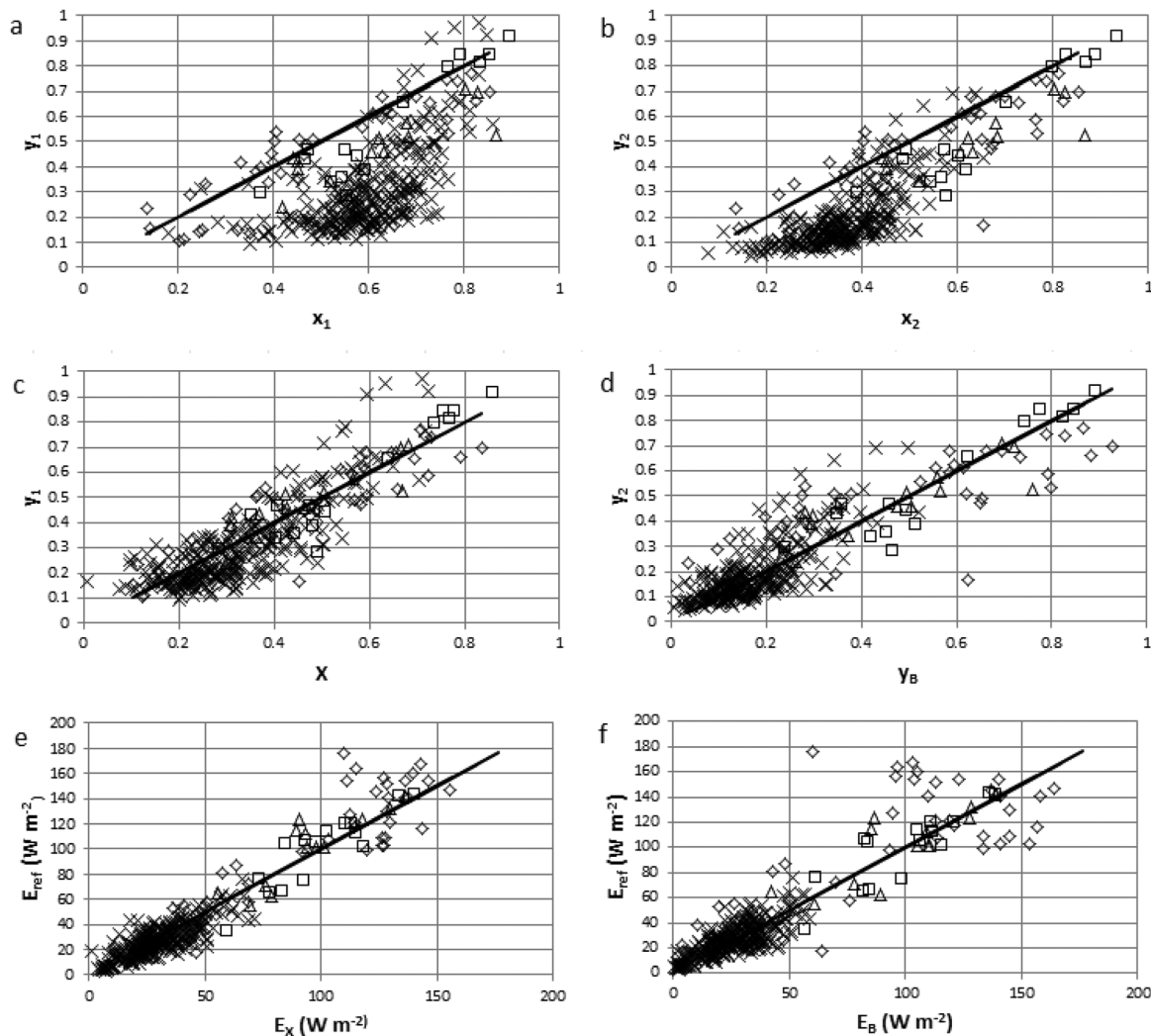


**Figure 1.** Results for all data sets. X's— BARCAS; Diamonds— FIFE87; Squares—FIFE89; Triangles—CASES. (a, c, and e; left column of graphs) Results using parameters that optimize equation (14). (b, d, and f; right column) Use parameters that optimize (5). Variables are defined in the text. The solid lines show the one-to-one relationship.

We identify a previously neglected problem, related to  $x_{min}$ , which can be resolved by rescaling the  $x$  axis in a graph like Figure 1a. Consider two hypothetical points on such a graph, both measured above the same landscape, but on different days. Both are located at  $x = 0.6$ , but one of them has  $x_{min} = 0.2$  and the other has  $x_{min} = 0.5$ . Measured in the  $x$  direction, the first point is thus half way between the points with coordinates  $(x_{min} = 0.2, 0)$  and  $(1, 1)$ . The other point is only one fifth of the way between  $(x_{min} = 0.5, 0)$  and  $(1, 1)$ , and thus should be closer to  $y = 0$  than the first point, even though both hypothetical points have the same value of  $x$ . To resolve this problem, the  $x_1$  axis of Figure 1a should be rescaled, replacing the  $x$  axis with  $X$ , as defined by (13) so that  $(X, y)$  always has the two limits  $(0, 0)$  and  $(1, 1)$ .

Figure 1c shows the results of this rescaling. Comparison of Figures 1a and 1c indicates, through a reduction in the scatter, that rescaling using (13) actually provides a better organization of the data than is available from Figure 1a. The reduction in scatter is also reflected by the fact that the correlation coefficient  $R$  between  $X$  and  $y_1$  is always greater with these data than the value of  $R$  between  $x_1$  and  $y_1$  ( $R = 0.89$  compared to  $0.83$  for FIFE87;  $0.94$  compared to  $0.93$  for FIFE89;  $0.88$  compared to  $0.84$  for CASES, and  $0.82$  compared to  $0.63$  for BARCAS). While the statistical significance of these individual correlations varies, overall,  $R$  values are greater between  $X$  and  $y_1$  than between  $x_1$  and  $y_1$ .

Comparing the position of individual data points in Figure 1a with the corresponding data points in Figure 1b, for the FIFE89 data, data points shifted only in the  $x$  direction, since  $\alpha$  (the only variable affecting  $x$  or  $y$

that was calibrated with this data set) only appears in  $x$ . For FIFE87 and CASES, data appear in the same place in Figures 1a and 1b, because the same value of  $\alpha$  optimizes both (5) and (14), as seen in Table 1. For all three of these experiments, correlations between  $x$  and  $y$  are the same in Figure 1a as they are in Figure 1b, because multiplying  $x$  by a constant (the ratio of the two values of  $\alpha$ ) does not change  $R$ . For the BARCAS data, shifts occurred in both the  $x$  and  $y$  directions, because  $m$  affects  $E_{pa}$ , which appears in both  $x$  and  $y$ .

Values of  $x_{min}$  and  $X$  can also be calculated using the  $\alpha$  and  $m$  values used in  $x_2$  and  $y_2$  rather than  $x_1$  and  $y_1$ . In either case, rescaling from  $x$  to  $X$  consistently yields higher values of  $R$  between  $X$  and  $y$  than between  $x$  and  $y$ . For example, when  $x_2$  on Figure 1b is rescaled as  $X$ , the correlation coefficients (see Table 1) between this  $X$  and  $y_2$  are higher than those between  $x_2$  and  $y_2$  (0.89 compared to 0.83 for FIFE87, 0.94 compared to 0.93 for FIFE89, 0.88 compared to 0.84 for CASES, and 0.83 compared to 0.71 for BARCAS). Furthermore, this improvement in correlation occurs also when the variables are calibrated by minimizing RMSD between estimated and reference values of the dimensionless evaporation rate  $y$  instead of  $E$  (results not shown). Note that  $\alpha$  does affect  $x_{min}$  (equation (12)), and therefore it can affect  $X$  and correlations between  $X$  and  $y$ .

The increased organization when rescaling with (13) is the primary finding of this study, and suggests that a CR should be built directly on the relationship between  $X$  and  $y$ , rather than  $x$  and  $y$ . But Figure 1c suggests a further hypothesis. The data points in Figure 1c are clustered around the line  $y = X$ . This motivates the proposal that a new CR can be expressed as  $y = X$  (equation (14)). Implications and alternatives will be addressed.

The comparison of the performance of  $E_X = y_1 * E_{pa1}$  from (14) with that of  $E_B = y_B * E_{pa2}$  from (5) is found in Table 1 and in Figures 1e and 1f. Correlations with  $E_{ref}$  are higher and RMSD values are lower using  $E_X$  compared to  $E_B$ , for all the data sets. Correlation coefficients between  $X$  and  $y_1$  (see Table 1 and Figure 1c) are greater than between  $y_B$  and  $y_2$  (see Table 1 and Figure 1d) for all the data sets. Neither the RMSD between  $X$  and  $y_1$  compared to  $y_B$  and  $y_2$ , nor the slopes and intercepts of the regression lines strongly favor either (5) or (14). Overall, however, (14) clearly performs better than (5). This is the case even though (5) has an additional parameter,  $c$ , which was adjusted to account for various degrees of asymmetry in the CR [Brutsaert, 2015]. This parameter was optimized individually for each data set. Equation (14) has no such parameter, although the height  $z$  in (10) is not fixed by physical necessity. Results using (5) to calculate  $y_B$  would be somewhat worse if the default value  $c = 0$  [Brutsaert, 2015] was used.

Comparison of the values of  $R$  in Table 1 shows that the correlation between  $y_B$  from (5) and reference values of  $y_2$  is nearly the same as the correlation between  $x_2$  and  $y_2$  for the FIFE87, FIFE89, and CASES data sets. While the value of  $R$  (Table 1) between  $y_B$  and  $y_2$  for the BARCAS sites ( $R = 0.75$ ) is greater than that between  $x_2$  and  $y_2$  ( $R = 0.71$ ), the value between  $X$  and  $y_2$  ( $R = 0.83$ ) is still greater. This is the case because (5) represents a single curve for each data set on Figure 1b. Rescaling  $x$  to  $X$  does not represent finding a new line or curve on Figure 1a (or 1b). Instead, it rearranges the data points, explaining more of the variability and resulting in reduced scatter. Finally, note that the rescaling requires individual estimates of  $x_{min}$  for each data point, while use of a constant value for  $x_{min}$  [Szilagyi et al., 2016] does not reorganize the data, reduce the scatter, or increase the correlation.

## 6. Discussion

The argument made here suggests that a CR should be formulated between  $X$  and  $y$  rather than  $x$  and  $y$ . The formulation pursued here can be summarized as  $y = X$ , where  $X = (x - x_{min}) / (1 - x_{min})$ . Given the care taken by Brutsaert [2015] to derive a very general CR, one would expect to find continuity between his derivation and the present results. With the proposed CR, the general relationship of Brutsaert [2015], namely the present equation (3), still holds, except now the function  $F$  is given by:

$$F = \frac{x_{min}}{1 - x_{min}} (1 - x) \tag{15}$$

In (3),  $F$  is construed to be a universal function only of  $1 - x$ ; here it is a function of both  $x_{min}$  and  $1 - x$ .

There is also continuity between the boundary conditions (BCs) suggested by Brutsaert [2015] and the proposed CR. As mentioned previously, he proposed the BCs: (i)  $y = 1$  at  $x = 1$ ; (ii)  $y = 0$  at  $x = 0$ ; (iii)  $dy/dx = 1$  at  $x = 1$ ; (iv)  $dy/dx = 0$  at  $x = 0$ . BC (i) is explicitly retained in this formulation because  $X = 1$  at  $x = 1$ . BC's (ii)

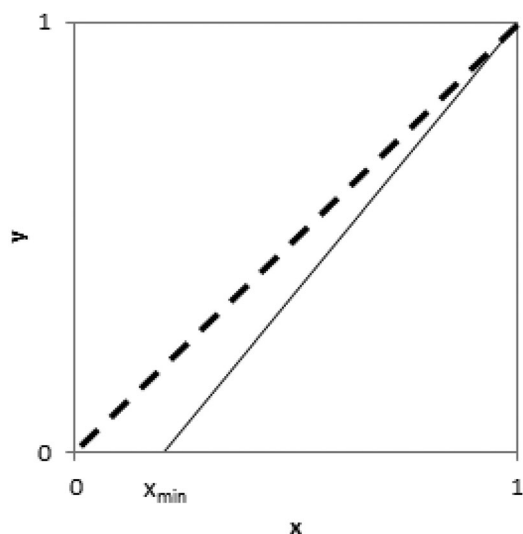


**Figure 2.** The proposed self-adjusting complementary relationship shown on an  $(x, y)$  graph, defined by a straight line connecting  $(x_{min}, 0)$  and  $(1, 1)$ . The dashed line represents  $y = x$ ; the solid line is equivalent to  $y = X = (x - x_{min}) / (1 - x_{min})$ , where  $x_{min}$  varies from day to day.

and (iv) are met with (14) if we specify  $y = 0$  for  $x < x_{min}$  so that both  $y$  and  $dy/dx$  are equal to zero at  $x = 0$ ; this situation is only hypothetical since  $x$  cannot be smaller than  $x_{min}$ . BC (iii) becomes  $dy/dX = 1$  or  $dy/dx = (1 - x_{min})^{-1}$  at  $X = x = 1$ , which is a small modification to  $dy/dx = 1$  at  $x = 1$ . To summarize, Brutsaert's [2015] BCs (i), (ii), and (iv) are essentially intact, while (iii) becomes  $dy/dX = 1$  or  $dy/dx = (1 - x_{min})^{-1}$  at  $X = x = 1$ .

Another way of explaining this CR (equation (14)) is to note that  $dy/dx = 1/(1 - x_{min})$  for all  $x_{min} \leq x \leq 1$ . That is,  $dy/dx$  does not depend on  $x$  but is a function only of  $x_{min}$ . This can be expressed using the familiar CR relationship [Brutsaert and Parlange, 1998; Kahler and Brutsaert, 2006]:

$$y = \frac{1+b}{b}x - \frac{1}{b} \tag{16}$$

where  $b$  has in the past been taken as a constant for a given site. Equation (16) has proved to be quite flexible when  $b$  has been taken as a constant for a given experiment [e.g., Brutsaert and Parlange,

1998; Kahler and Brutsaert, 2006; Pettijohn and Salvucci, 2009; Huntington et al., 2011], but in this new CR,  $b$  must be found for each daily (or 10 day averaged) data point as  $b = (1 - x_{min})/x_{min}$ . Figure 2 shows what this looks like on an  $x$ - $y$  graph. The dashed line representing  $y = x$  corresponds to  $x_{min} = 0$  and  $b \rightarrow \infty$ . The solid line on Figure 2 represents the new CR for a single data point. It can be seen that days (or 10 day averages) having larger values of  $x_{min}$  will exhibit a more vertical CR line (the solid line on Figure 2), corresponding to a smaller value of  $b$ , and resulting in smaller values of  $y$  for a given  $x$ . Note that a fixed value of  $b$  for a given experiment cannot reorganize the data in the way equation (14) can. In fact, the correlation coefficient for any fixed value of  $b$  is the same as that between  $x$  and  $y$ , and Table 1 shows that  $R$  between  $x$  and  $y$  is smaller than between  $X$  and  $y$ .

The data considered here seem to support writing the CR as  $y = X$  (equation (14)). However, as noted by Brutsaert [2015], some flexibility in CR formulations may be needed to accommodate a range of regional field conditions. Adding flexibility to (14) would align with the thrust of this paper, provided the CR is based on the rescaled  $x$  axis. For example, a great deal of flexibility is possible with a CR equation of the form:

$$y = a_0 + a_1X + a_2X^2 + a_3X^3 \tag{17}$$

in which the coefficients can be assigned to meet various boundary conditions. When  $a_0 = a_2 = a_3 = 0$ , and  $a_1 = 1$ , (17) reduces to (14). Four BCs are needed to evaluate the coefficients [Brutsaert, 2015]. We might specify these BCs: (i)  $y = 0$  at  $X = 0$ ; (ii)  $y = 1$  at  $X = 1$ ; (iii)  $dy/dX = s$  at  $X = 1$ ; and (iv)  $dy/dX = \sigma$  at  $X = 0$ . BCs (iii) and (iv) define  $s$  and  $\sigma$ , respectively. This results in:  $a_0 = 0$ ;  $a_1 = \sigma$ ;  $a_2 = 3 - s - 2\sigma$ ; and  $a_3 = -2 + s + \sigma$ . Values of  $s$  and  $\sigma$  must be chosen such that  $y \leq x$ , and  $y \geq 0$  for  $x_{min} \leq x \leq 1$ ; these values may be selected on physical grounds or through calibration. Since (14) adequately represents the present data, (17) will not be applied here.

### 7. Conclusions

The complementary relationship (CR) has been rescaled by defining  $x_{min}$  as the value of  $x = E_{po}/E_{pa}$  at which  $y = E/E_{pa}$  goes to zero. By calculating  $x_{min}$  with (12), the  $x$  axis can be rescaled to  $X = (x - x_{min}) / (1 - x_{min})$ . The reduced scatter shown in the rescaled CR (Figure 1c) cannot be represented by a single curve on the  $x$ - $y$  axes, even for a single experimental site. Rather, each data point has its own  $x_{min}$ , defining the CR for that data point. The present data suggest the CR can be expressed as  $y = X$  (equation (14)). Calculation of  $x_{min}$  requires no additional data beyond those required to calculate evaporation from the Penman [1948]

equation as expressed in (7) and (8). Although the *Priestley and Taylor* [1972] parameter has been calibrated for use here, this poses no additional requirement beyond those for any application of the Advection-Aridity class of CR methods.

This rescaling has the potential to explain much of the variability in the value of  $b$  observed by, for example, *Kahler and Brutsaert* [2006], *Szilagyi* [2007], *Pettijohn and Salvucci* [2009], and *Huntington et al.* [2011]. It also has the potential to reduce the scatter within individual data sets.

To summarize:

1. A method has been proposed to estimate  $E_{pa}$  under conditions where  $E$  goes to zero while  $E_{po}$  is greater than zero. This value is denoted  $E_{pads}$  (equation (10)).
2. This value of  $E_{pads}$  can be used to find the minimum value of  $x = E_{po}/E_{pa}$  attainable as  $E$  goes to zero on a given day (equation (12)). This value is denoted  $x_{min}$ .
3. The complementary relationship, typically expressed by  $y = f_1(x)$ , can be rescaled as  $y = f_2(X)$  where  $X = (x - x_{min})/(1 - x_{min})$ , where  $f_1$  and  $f_2$  are functions of  $x$  and  $X$ , respectively.
4. Plotting experimental data from FIFE87, FIFE89, CASES, and BARCAS resulted in reduced scatter in plots of  $X$  versus  $y$ , compared to  $x$  versus  $y$ .
5. With all the data sets, the  $(X, y)$  data fall near the line  $y = X$ .
6. The CR  $y = X$  better predicts measured  $E$  values overall than *Brutsaert's* [2015] equation (5), even when  $\alpha$  and  $c$  are optimized for his equation.

The new  $y = X$  formulation maintains considerable continuity with the reasoning behind the general CR derived by *Brutsaert* [2015]. The physical constraints reflected in his boundary conditions are maintained, although their mathematical expressions are modified.

Other possible functional forms of the CR, such as (17), should consider  $y$  to be a function of  $X$ , rather than  $x$ , in order to take advantage of the reduced scatter provided by this rescaling of the  $x$  axis.

#### Acknowledgments

This manuscript benefited greatly from comments and suggestions from two anonymous reviewers and the associate editor. Data from FIFE 1987 and 1989 are available from <https://daac.ornl.gov/FIFE/>. Data from CASES are available from <http://data.eol.ucar.edu/codiac/dss/id=20.05> (doi:10.5065/D6377735). Data from BARCAS are available through <http://nevada.usgs.gov/water/et/>.

#### References

- Allen, R. G., L. S. Pereira, D. Raes, and M. Smith (1998), Crop evapotranspiration: Guidelines for computing crop water requirements, FAO Irrig. Drain. Pap. 56, 300 pp., Food and Agric. Organ., Rome, Italy.
- Aminzadeh, M., M. L. Roderick, and D. Or (2016), A generalized complementary relationship between actual and potential evaporation defined by a reference surface temperature, *Water Resour. Res.*, 52, 385–406, doi:10.1002/2015WR017969.
- Bastiaanssen, W. G. M., M. Menenti, R. A. Feddes, and A. A. M. Holtslag (1998), A remote sensing surface energy balance algorithm for land (SEBAL): 1. Formulation, *J. Hydrol.*, 212–213, 198–212.
- Bouchet, R. J. (1963), Evapotranspiration réelle, évapotranspiration potentielle, et production agricole, *Ann. Agron.*, 14, 743–824.
- Brutsaert, W. (1982), *Evaporation into the Atmosphere: Theory, History, and Applications*, 299 pp., D. Reidel, Boston, Mass.
- Brutsaert, W. (2005), *Hydrology: An Introduction*, Cambridge Univ. Press, N. Y.
- Brutsaert, W. (2015), A generalized complementary principle with physical constraints for land-surface evaporation, *Water Resour. Res.*, 51, 8087–8093, doi:10.1002/2015WR017720.
- Brutsaert, W., and M. B. Parlange (1998), Hydrologic cycle explains the evaporation paradox, *Nature*, 396(5), 300.
- Brutsaert, W., and H. Stricker (1979), An advection-aridity approach to estimate actual regional evapotranspiration, *Water Resour. Res.*, 15, 443–450, doi:10.1029/WR015i002p00443.
- Crago, R., and R. Crowley (2005), Complementary relationships for near-instantaneous evaporation, *J. Hydrol.*, 300, 199–211.
- Crago, R., and A. Suleiman (2005), Heat flux parameterization for sparse and dense grasslands with the Analytical Land Atmosphere Radiometer Model (ALARM), *Boundary Layer Meteorol.*, 114, 557–572.
- Crago, R., and R. Qualls (2013), The value of intuitive concepts in evaporation research, *Water Resour. Res.*, 49, 6100–6104, doi:10.1002/wrcr.20420.
- Dingman, S. L. (2015) *Physical Hydrology*, 3rd ed., 643 pp., Waveland Press, Long Grove, Ill.
- Granger, R. J. (1989) A complementary relationship approach for evaporation from nonsaturated surfaces, *J. Hydrol.*, 111(1–4), 31–38.
- Han, S., H. Hu, and F. Tian (2012), A nonlinear function approach for the normalized complementary relationship evaporation model, *Hydrol. Processes*, 26(26), 3973–3981.
- Hobbins, M. T., A. Wood, D. J. McEvoy, J. L. Huntington, C. Morton, M. Anderson and C. Hain (2016), The evaporative demand drought index. Part I: Linking drought evolution to variations in evaporative demand, *J. Hydrometeorol.*, 17, 1745–1761.
- Huntington, J. L., J. Szilagyi, S. W. Tyler, and G. M. Pohl (2011), Evaluating the complementary relationship for estimating evapotranspiration from arid shrublands, *Water Resour. Res.*, 47, W05533, doi:10.1029/2010WR009874.
- Kahler, D. M., and W. Brutsaert (2006), Complementary relationship between daily evaporation in the environment and pan evaporation, *Water Resour. Res.*, 42, W05413, doi:10.1029/2005WR004541.
- McEvoy, D. J., J. L. Huntington, M. T. Hobbins, A. Wood, C. Morton, M. Anderson, and C. Hain (2016), The evaporative demand drought index. Part II: CONUS-wide assessment against common drought indicators, *J. Hydrometeorol.*, 17, 1763–1779.
- Monteith, J. L. and M. H. Unsworth (2013), *Principles of Environmental Physics: Plants, Animals, and the Atmosphere*, 4th ed., 401 pp., Academic, Boston, Mass.
- Moreo, M. T., R. J. Lacznik, and D. I. Stannard (2007), Evapotranspiration rate measurements of vegetation typical of ground-water discharge areas in the Basin and Range carbonate-rock aquifer system, Nevada and Utah, September 2005–August 2006, U.S. Geol. Surv. Sci. Invest. Rep., 2007-5078, 36 pp.

- Morton, F. (1983), Operational estimates of areal evapotranspiration, *J. Hydrol.*, *66*, 1–76.
- Nishida, K., R. R. Nemani, S. W. Running, and J. M. Glassy (2003), An operational remote sensing algorithm of land surface evaporation, *J. Geophys. Res.*, *108*(D9), 4270, doi:10.1029/2002JD002062.
- Penman, H. L. (1948), Natural evaporation from open water, bare soil, and grass, *Proc. R. Soc. London Ser. A*, *193*, 120–146.
- Pettijohn, J. C., and G. D. Salvucci (2009), A new two-dimensional physical basis for the complementary relation between terrestrial and pan evaporation, *J. Hydrometeorol.*, *10*, 565–574, doi:10.1175/2008JHM1026.1.
- Priestley, C. H. B., and R. J. Taylor (1972), On the assessment of surface heat flux and evaporation using large-scale parameters, *Mon. Weather Rev.*, *100*, 81–92.
- Qualls, R. J., and H. Gultekin (1997), Influence of components of the advection-aridity approach on evapotranspiration estimation, *J. Hydrol.*, *199*, 3–12.
- Ramirez, J. A., M. T. Hobbins, and T. C. Brown (2005), Observational evidence of the complementary relationship in regional evaporation lends strong support for *Bouchet's* hypothesis, *Geophys. Res. Lett.*, *32*, L15401, doi:10.1029/2005GL023549.
- Roderick, M. L., M. T. Hobbins, and G. D. Farquhar (2009a), Pan evaporation trends and the terrestrial water balance. I. Principles and Observations, *Geogr. Compass*, *3*(2), 746–760, doi:10.1111/j.1749-8198.2008.00213.x.
- Roderick, M. L., M. T. Hobbins, and G. D. Farquhar (2009b), Pan evaporation trends and the terrestrial water balance. II. Energy balance and interpretation, *Geogr. Compass*, *3*(2), 761–780.
- Sellers, P. (1994), Surface Flux Baseline 92 Derived (FIFE): Data set, Oak Ridge Natl. Lab. Distrib. Active Arch. Cent., Oak Ridge, Tenn., doi:10.3334/ORNLDAAC/121. [Available at <http://www.daac.ornl.gov>.]
- Sellers, P. J., F. G. Hall, G. Asrar, D. E. Strebel, and R. E. Murphy (1992), An overview of the First International Satellite Land Surface Climatology Project (ISLSP) Field Experiment (FIFE), *J. Geophys. Res.*, *97*, 18,345–18,371.
- Shuttleworth, J. W., and R. J. Gurney (1990), The theoretical relationship between foliage temperature and canopy resistance in sparse crops, *Q. J. R. Meteorol. Soc.*, *116*, 497–519, doi:10.1002/qj.49711649213.
- Shuttleworth, J. W., and J. S. Wallace (1985), Evaporation from sparse crops and energy combination theory, *Q. J. R. Meteorol. Soc.*, *111*, 839–855, doi:10.1256/smsqj.46909.
- Szilagyi, J. (2007), On the inherent asymmetric nature of the complementary relationship of evaporation, *Geophys. Res. Lett.*, *34*, L02405, doi:10.1029/2006GL028708.
- Szilagyi, J. (2014), Temperature corrections in the Priestley-Taylor equation of evaporation, *J. Hydrol.*, *519*, 455–464.
- Szilagyi, J. (2015), Complementary-relationship-based 30 year normal (1981–2010) of monthly latent heat fluxes across the contiguous United States, *Water Resour. Res.*, *51*, 9367–9377, doi:10.1002/2015WR017693.
- Szilagyi, J., and J. Jozsa (2008), New findings about the complementary relationship-based evaporation estimation methods, *J. Hydrol.*, *354*(1–4), 171–186.
- Szilagyi, J., and A. Schepers (2014), Coupled heat and vapor transport: The thermostat effect of a freely evaporating land surface, *Geophys. Res. Lett.*, *41*, 435–441, doi:10.1002/2013GL058979.
- Szilagyi, J., R. Crago, and R. Qualls (2016), Testing the generalized complementary relationship of evaporation with continental-scale long-term water-balance data, *J. Hydrol.*, *540*, 914–922.